Pyrene: Hydrogenation, hydrogen evolution, and π-band model

Jakob Arendt Rasmussen,[1] Graeme Henkelman,[2] and Bjørk Hammer[1,a)]
[1]*Interdisciplinary Nanoscience Center (iNANO) and Department of Physics and Astronomy, Ny Munkegade, Building 1520, Aarhus University, DK-8000 Aarhus C, Denmark*
[2]*Department of Chemistry and Biochemistry, The University of Texas at Austin, Austin, Texas 78712-0165, USA*

(Received 12 November 2010; accepted 16 February 2011; published online 29 April 2011)

We present a theoretical investigation of the hydrogenation of pyrene and of the subsequent molecular hydrogen evolution. Using density functional theory (DFT) at the GGA-PBE level, the chemical binding of atomic hydrogen to pyrene is found to be exothermic by up to 1.6 eV with a strong site dependence. The edge C atoms are found most reactive. The barrier for the formation of the hydrogen–pyrene bond is small, down to 0.06 eV. A second hydrogen binds barrierless at many sites. The most stable structure of dihydrogenpyrene is more stable by 0.64 eV than pyrene plus a molecular hydrogen molecule and a large barrier of 3.7 eV for the molecular hydrogen evolution is found. Using a simple tight-binding model we demonstrate that the projected density of π-states can be used to predict the most stable binding sites for hydrogen atoms and the model is used to investigate the most favorable binding sites on more hydrogenated pyrene molecules and on coronene. Some of the DFT calculations were complemented with hybrid-DFT (PBE0) showing a general agreement between the DFT and hybrid-DFT results. © *2011 American Institute of Physics*. [doi:10.1063/1.3563632]

I. INTRODUCTION

In the interstellar medium, molecular hydrogen is generally believed to form on the surface of dust grains.[1,2] Laboratory experiments have, however, shown that reactions between physisorbed H atoms on dust grain surfaces are only efficient at temperatures below 20 K.[3] In regions with higher temperatures, such as, e.g., photo dissociation regions, other possible routes to molecular hydrogen formation must be invoked. Polycyclic aromatic hydrocarbons (PAHs) have been proposed as a possible catalyst for H_2 formation in these regions.[4,5] The consideration of PAHs in this context follows naturally from their high abundance in the interstellar medium. In fact, it is estimated that up to 15% of interstellar carbon is bound in PAHs making them the single most abundant group of organic species in the interstellar medium.[6] The study of the chemistry of PAHs is consequently highly representative for organic chemistry going on in the interstellar medium thereby rendering it the model system of choice.

A number of theoretical studies of hydrogenation of PAHs have been performed[4,5,7,8] showing propensity for strong H–PAH bond formation especially at the edge of the PAHs. This renders the study of hydrogen interaction with PAHs complementary to the immensely studied topic of hydrogen adsorption at graphene and graphite surfaces[9–26] and means that PAHs can be considered to represent finite model systems for hydrogen on defected graphite and graphene—an idea already explored by several researchers.[27–29]

In the present work, we aim at establishing the reactivity of a small PAH, pyrene, investigating systematically at the density functional theory (DFT) level the binding of one and two hydrogen atoms to the pyrene and mapping the barriers for the evolution of molecular hydrogen. Our systematics dictates that all conceivable singly hydrogenated pyrene, H-pyrene, molecules and doubly hydrogenated pyrene, dihydrogenpyrene, molecules be described in full at the DFT level. This in turn provides a database for testing if simpler theoretical models may predict the preferred H binding sites on pyrene. We find that evaluating in a tight-binding model the energy center, ε_π, of the occupied density of π-states projected at each carbon site prior to H binding provides a powerful parameter for predicting the hydrogen binding site preference. The ε_π parameter is further tested on selected binding situations for hydrogen interacting with hydrogenated pyrene and coronene.

At present, most previous DFT calculations on hydrogenated PAHs and hydrogen adsorption on graphite/graphene have been performed in the generalized gradient approximation (GGA). Since binding with a hydrogen atom modifies delocalized carbon π-states into localized C–H bonds a relevant improvement to the present type of calculations would be the use of hybrid-DFT where a certain amount of Hartree–Fock (HF) exchange is taken into account.[30,31] Hybrid functionals are believed to describe localized bonding better than GGA functionals and to significantly improve the calculation of atomization energies compared to the GGA-DFT.[31] Inclusion of 43% exact exchange has further been shown to improve the kinetics of hydrogen transfer reactions.[32] In our work, however, comparing reaction energies and energy barriers at the DFT and hybrid-DFT level only shows small differences.

The paper is outlined as follows: details concerning the calculations are described in Sec. II; in Sec. III the DFT results for binding one or two hydrogen atoms to pyrene are presented. In Sec. IV, the π-band center model is introduced

a)Author to whom correspondence should be addressed. Electronic mail: hammer@phys.au.dk.

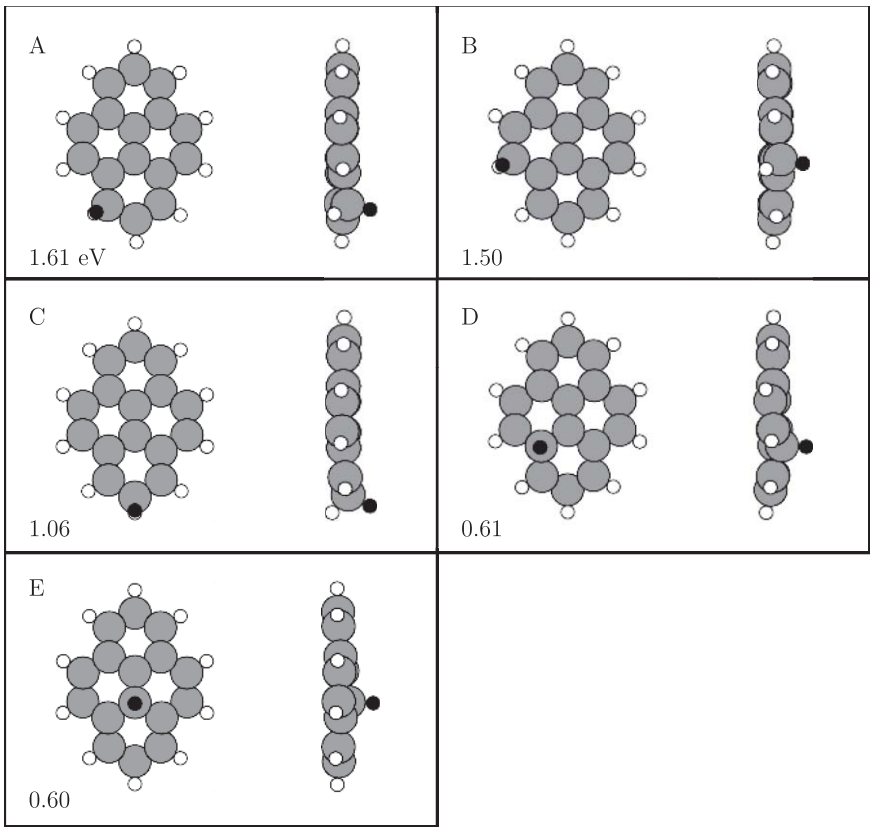

FIG. 1. Hydrogen monomer configurations on pyrene. The dark sphere marks the position of the extra H atom. Numbers are the binding energies in eV.

thereby rationalizing the DFT results and predicting further ones. Section V deals with comparing DFT and hybrid-DFT. Finally, Sec. VI provides a conclusion.

II. METHOD

The calculations were performed with the GPAW code[33,34]—a real space grid implementation of the projector augmented wave method.[35] Three different approximations for the exchange–correlation interaction have been applied: the generalized gradient approximation by Perdew, Burke, and Ernzerhof (PBE),[36] the corresponding hybrid (PBE0),[31,37] and finally pure Hartree–Fock (EXX) with exact exchange and no correlation. All used structures are optimized with the PBE exchange correlation functional using a quasi-Newton optimization routine. A grid spacing of 0.16 Å was used and a nonperiodic cubic computational cell of dimensions $15\times15\times15$ Å^3. The calculations were converged with respect to cell size and grid spacing. All calculations were performed spin-polarized. Barriers and potential energy profiles were determined using the nudged elastic band method.[38,39] Care was taken when assigning the initial magnetic moments along the Eley–Rideal (ER) pathways. Specifically, the adiabatic paths were found using initial magnetic moments from the initial situation before the H abstraction characterized by very small magnetic moments for the pyrene skeleton and using guesses of 1 μ_B and -1 μ_B for the excess hydrogen atoms. The reaction coordinate in figures showing potential energy profiles is defined following Mortensen *et al.*[40] as

$$s_n = \sum_{i=1}^{n-1} |\Gamma_{i+1} - \Gamma_i| , \quad (1)$$

where Γ is a vector containing the coordinates of all the atoms. The indices denote which image along the path is under consideration. In this way s is the total displacement of all atoms along the path from the initial state at $s = 0$. Contributions to s will primary be the movement of hydrogen atoms.

Some hydrogen binding energies and reaction energy barriers were checked with the plane wave DFT code VASP (Refs. 41–43) using a kinetic energy cutoff of 400 eV. The calculations were done with Γ **k**-point sampling and converged with respect to repeated super cell size, leading to the usage of a super cell of $14\times14\times14$ Å^3 for all calculations reported herein. The binding energies were again determined with the same three methods (PBE, PBE0, and EXX) using the PBE-structures but also with the self-consistently relaxed structures for PBE0.

III. RESULTS

A. Singly hydrogenated pyrene

Figure 1 shows the five distinct positions in which one hydrogen atom can bind on pyrene—the rest follows by symmetry. These singly hydrogenated pyrene molecules will in the following be referred to as hydrogen monomers. The binding energies of the five monomers calculated in the PBE

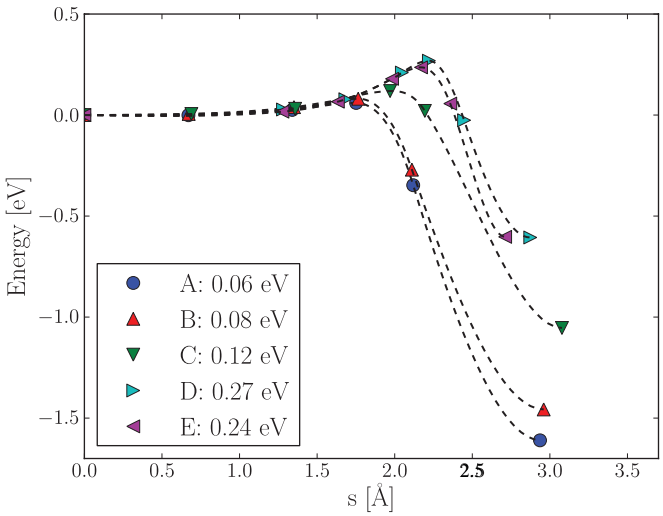

FIG. 2. Potential energy profiles for the binding of one hydrogen monomer on pyrene. The barriers are given in the legend.

approximation with GPAW are given in the figure, and the configurations are ordered with respect to binding energies with the most stable configuration first.

The three most stable monomers [Figs. 1(a)–1(c)] have binding energies ranging from 1.0 to 1.6 eV and have in common that the carbon atom at which the hydrogen binds are pyrene edge sites for which the carbon atoms only coordinate to two other carbon atoms. The two carbon atoms in the interior of the pyrene molecule bind a hydrogen atom with 0.6 eV.

Upon binding a hydrogen atom the carbon skeleton relaxes. This has the largest impact for the interior positions (D and E) where the carbon atom puckers approximately 0.4 Å out of the molecular plane. For edge sites (A–C) the effect is a factor of 2 smaller, i.e., approximately 0.2 Å.

The potential energy profiles during the formation of the chemical bond between hydrogen and pyrene at the five different positions are shown in Fig. 2 where also the corresponding reaction energy barriers are quoted. Zero along the abscissa is with the incoming hydrogen atom around 4 Å above the chemisorption position. The barrier of 0.06 eV for binding the most stable hydrogen monomer on pyrene is in good agreement with previous results for hydrogen on coronene where the barrier for forming the most stable configuration was also determined to around 0.06 eV.[5] We note that tunneling could contribute to the reaction rate for bonding a hydrogen atom to a PAH.[44]

B. Doubly hydrogenated pyrene

We next consider the situation that the pyrene is doubly hydrogenated. Since our focus is on the excess hydrogen atoms of such compounds, we shall refer to these dihydrogenpyrene species as dimers (of hydrogen bonded to pyrene) and label them according to the positions of the two excess hydrogen atoms. Considering each carbon atom a distinct binding site, one can construct 43 symmetry inequivalent hydrogen dimers on pyrene. This includes both one- and two-sided hydrogenation. We performed DFT calculations for all of them—except for two for which it turned out to be impossible to reach convergence—thereby identifying unequivocally the most stable dimer configurations. The nine very most stable ones are depicted in Fig. 3 where also the combined binding energies (and stabilization energies; see Sec. IV) of the two H atoms are reported. The dimers are named by their monomers (A–E) and then a number of primes depending on the orientation of the monomers with respect to each other. Placing the most stable monomer in the lower left corner of the molecule there will be: no primes if the second monomer is in the same part; one prime if the second monomer is in the upper left corner of the molecule; two primes if the second monomer is in the upper right corner of the molecule, and three primes if the second monomer is in the lower right part of the molecule.

The structural relaxation of the carbon skeleton for dimers AB″, AA′, AA″, and AB′ is similar to that of the monomer edge configurations, i.e., a puckering of up to 0.2 Å. The paradimers (AD‴ and BE′) show a puckering of up to 0.5 Å. The orthodimers (BB′, AC, and AD) show the characteristic tilt of the carbon–carbon bond also seen for coronene.[5]

Given the nine dimers in Fig. 3 we investigated the potential energy curves for the formation of these dimers by attachment of one hydrogen atom to a pyrene already accommodating one hydrogen atom. With nine dimers, there are 18 possible hydrogen attachment events, but three turn out to be symmetry related leaving 15 distinct potential energy curves that were all calculated. None of the reaction events involved a reaction energy barrier according to these investigations. An example of one such potential energy curve is shown in Fig. 4 for the reaction leading to the formation of the most stable dimer. The incoming hydrogen atom starts out approximately 4.4 Å above the molecular plane.

The potential energy curve in Fig. 4 shows that the dimer formation happens spontaneously. This is further in good agreement with investigations of hydrogen-dimers on the graphite(0001)-surface which suggest barrierless adsorption at certain positions for the second hydrogen (preferential sticking)[17,25,29] and co-bonding of hydrogen atoms on the coronene molecule.[5]

C. Molecular hydrogen formation

There are two conceivable ways to form molecular hydrogen from PAHs or hydrogenated PAHs. Either hydrogen on a PAH is abstracted by an impinging atomic hydrogen atom, or two hydrogen atoms on a PAH become activated and overcome the barrier for recombination and desorption. Adopting the terminology of surface science we shall be referring to the two reaction scenarios as either the ER abstraction pathway or the Langmuir–Hinshelwood recombinative desorption (LH) pathway.

The potential energy profiles for the ER pathway of hydrogen position A and E are shown in Fig. 5(a). For position A the incoming hydrogen atom starts out around 4 Å above the molecular plane—for position E it is 4.5 Å. These

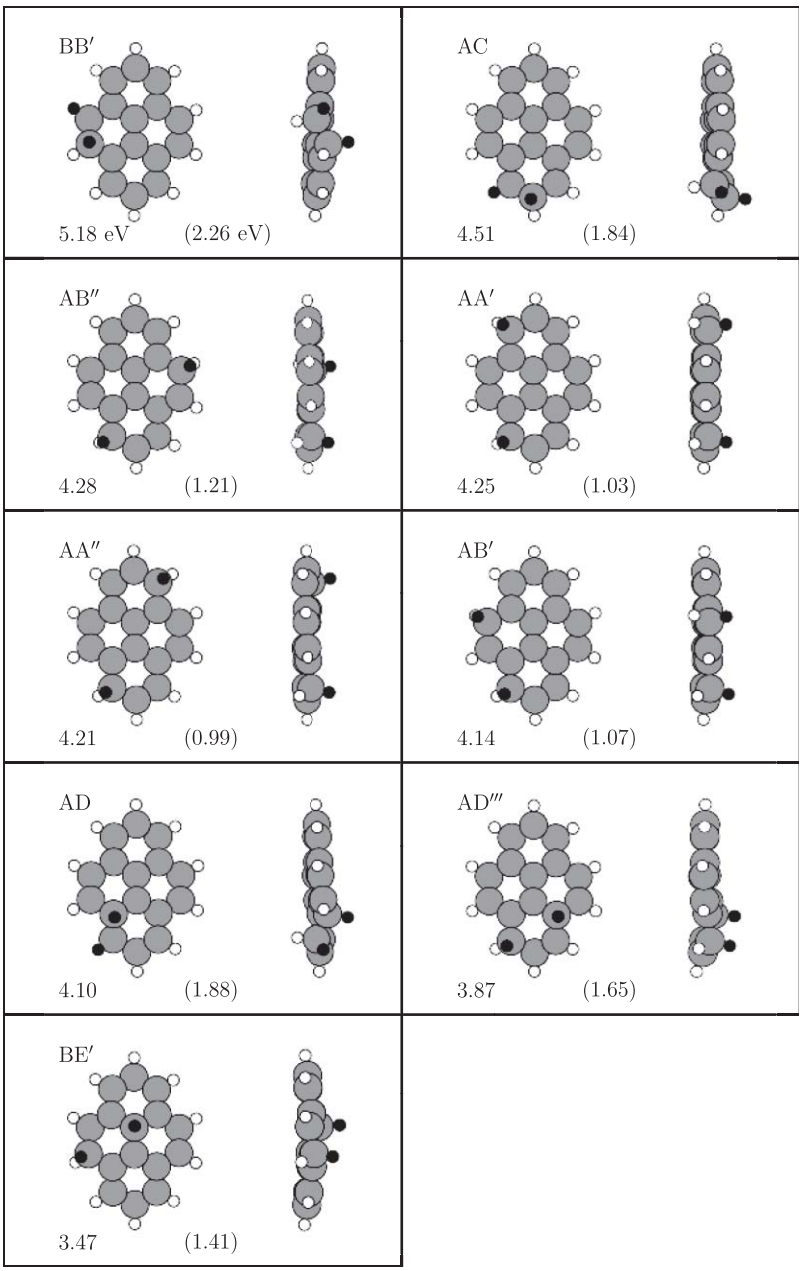

FIG. 3. The nine most stable hydrogen dimer configurations on pyrene. Total binding energies and stabilization energies in parentheses (see Eq. (2)) are given in eV.

two positions have been chosen because they are conceptually different—position A being an edge site and position E an interior site. Furthermore, the two positions represent the two extremes of hydrogen monomer binding on pyrene. Generally, there is a very small barrier toward hydrogen formation along such ER paths, i.e., 50 meV for position A and 80 meV for position E. Comparably small barriers for similar reactions have been reported elsewhere [13 meV (Ref. 45) and few tens of meV (Ref. 12)]. The final potential energy in Fig. 5(a) is −4.54 eV and represents pyrene $+H_2$ with respect to pyrene $+2 \times$ H meaning that the H_2 formation energy (less zero-point energy effects) is 4.54 eV with our level of DFT modeling.

Turning to the LH mechanism dimer BB′—the most stable dimer—can be desorbed with a barrier of 4.5 eV. This reaction is shown with blue triangles in Fig. 5(b). With red squares in the same figure is shown the potential energy profile for the desorption of dimer AD‴ for which the barrier is 1.4 eV. Transferring the International Union of Pure and Applied Chemists (IUPAC) nomenclature for substituents on an aromatic ring to the excess hydrogens on the aromatic rings in pyrene these two dimers may be characterized as ortho- (in BB′ the H atoms are nearest neighbors in the carbon hexagon) and paradimers (in AD‴ the H atoms are at opposite sites in the carbon hexagon) and they thereby represent two different types of hydrogen dimers. The ordering of these barriers conform well with the work done on graphene where desorption is expected to occur from the paraconfiguration with a barrier of 1.4 eV while the orthodimer is reported to be associated with a large, 2.5 eV, barrier for the direct recombina-

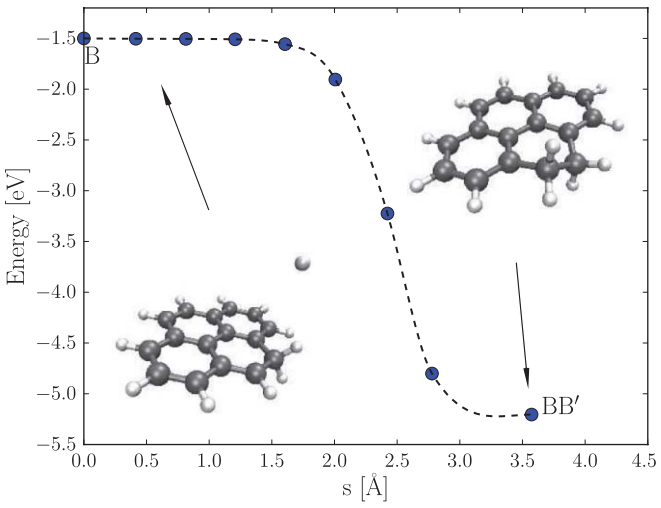

FIG. 4. Potential energy profile for forming the most stable dimer (BB′) from one monomer (B).

tive desorption.[18] The very large barrier of 4.5 eV for the BB′ dimer should be compared to the barrier for diffusion into the closest related paradimer BE′. This diffusion happens via the metadimer, BD′, with a barrier of 3.7 eV. From the BE′ dimer desorption can then happen with a barrier of 1.4 eV thereby lowering the overall barrier for desorption of the BB′ dimer

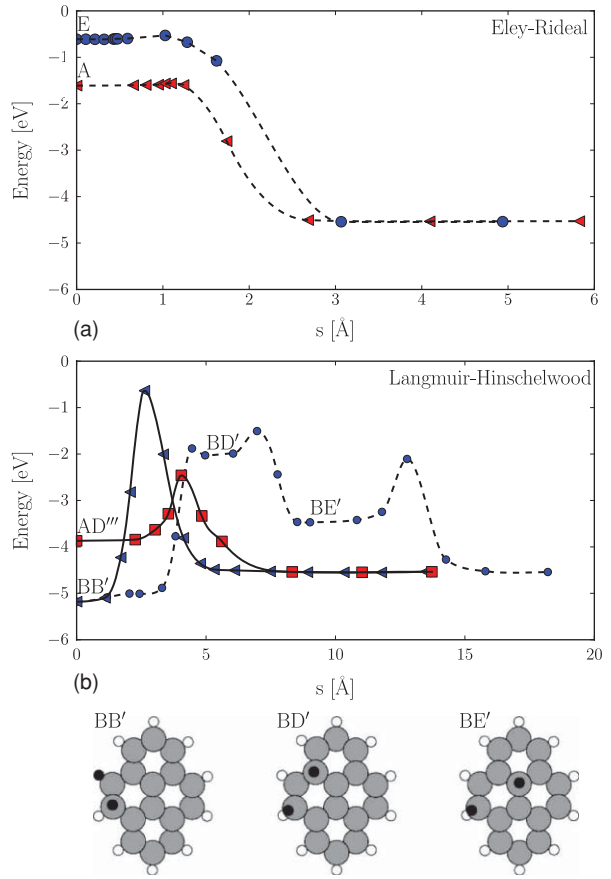

FIG. 5. Potential energy profiles for (a): the Eley–Rideal abstraction of a hydrogen atom in position A and E and (b): the Langmuir–Hinshelwood mechanism for dimers BB′ and AD‴ (full lines) and the diffusion of dimer BB′ through dimer BD′ into dimer BE′ (dashed line).

with 0.8 eV. The combined diffusion and desorption is shown with blue circles and a dashed line in Fig. 5(b). The involved configurations are drawn below the figure.

Looking at Fig. 4 it is seen that the addition of hydrogen number two proceeds without a barrier and is associated with an energy gain of 3.68 eV (= 5.18 eV binding of BB′ minus 1.50 eV binding of B). Consequently, it will cost 3.68 eV to remove one hydrogen from dimer BB′. The removed hydrogen could then extract the other hydrogen via an ER abstraction which were shown to proceed almost without a barrier. By chance similar two step H_2 desorption events involving the desorption of one hydrogen atom and an ER step were found for dimer AC with a barrier of 2.9 eV (corresponding to 4.51 eV binding of AC minus 1.61 eV binding of A) and dimer AD with a barrier of 2.5 eV (4.10 eV binding of AD minus 1.61 eV binding of A) instead of the LH mechanism.

The very large barrier for forming H_2 from the BB′ dimer is accompanied by a positive (i.e., endothermic) reaction energy of 0.64 eV [−4.54−(−5.18) eV], reflecting that the initial state of the BB′ dimer, i.e., doubly hydrogenated pyrene, is indeed more stable than the final state of pyrene plus molecular hydrogen.

Considering the very large barriers for the LH reaction we are aware that there could possibly exist lower barriers. However, the general picture appears to be that the barriers are exceedingly high for the ortho-type dimers (BB′, AC, and AD) but smaller for the paradimers (AD‴ and BE′). Yet, even these barriers appear large in comparison with the minute barriers for the ER reaction.

IV. DISCUSSION AND π-BAND CENTER MODEL

A. Stability of monomers and dimers

As already noted, the strongest binding energies of hydrogen at pyrene are obtained at the edge of the pyrene molecule. The binding of 1.6 eV found in this work using the GGA-PBE functional compares well with the GGA-PW91 calculation of 1.45 eV for the binding of edge-bound hydrogen on the larger PAH coronene as reported by Rauls and Hornekær.[5] The much weaker binding of 0.6 eV in the interior of the pyrene is in good agreement with the binding energy of 0.64 eV (GGA-PW91) calculated by Ferro *et al.*[13] and further conforms with the weaker 0.7 eV binding (GGA-PW91) at the interior of coronene[5] and with the 0.8 eV (GGA-PW91) binding reported by Sljivancanin *et al.*[25] for hydrogen binding at the basal plane of graphene.

The six most stable hydrogen dimers have in common that they are all edge configurations. That is, none of them contain a hydrogen atom bound in the interior (sites D and E). The seventh and eighth most stable dimers (AD and AD‴ in Fig. 3) contain hydrogen atoms bound in site D near the interior and the ninth dimer (BE′) is the first to have a hydrogen atom bound on the interior site E. The most stable hydrogen dimer for which both hydrogens are at interior sites (not shown) interestingly have the two hydrogen atoms on

opposite sites, as has also been reported to be energetically preferred for the hydrogen dimer on graphene.[46]

Looking at Fig. 3 it can be seen that dimers where the two hydrogen atoms are bound to the same carbon hexagon have a large degree of reconstruction of the carbon skeleton. For the orthodimers (BB′, AC, and AD) this is the characteristic twist of the carbon–carbon bond out of the molecular plane. For the paradimers (AD‴ and BE′) the carbon atoms only puckers out of the molecular plane. The puckering is even more pronounced for the monomers where monomers E and D (Fig. 1) are less stable and have a larger reconstruction.

In order to discuss further the interaction between the extra H atoms binding to pyrene, we have evaluated the stabilization energies defined as

$$E_{\text{stab}} = E_{\text{dim}}(XY) - E_{\text{mon}}(X) - E_{\text{mon}}(Y). \tag{2}$$

The stabilization energy, E_{stab}, measures the deviation of the potential energy, $E_{\text{dim}}(XY)$, of dimer XY from the sum of the potential energies, E_{mon}, of the two monomers X and Y that the dimer is comprised of. The stabilization energies are given in parentheses in Fig. 3. They are seen to be rather dependent on the distance between the extra hydrogen atoms on the pyrene.

The dimers can be divided into three groups: ortho-, para-, and extended dimers. For the ortho- and paradimers both excess hydrogen atoms are situated on the same carbon hexagon and the distance between them is therefore small as compared to the extended dimers where the hydrogen atoms are situated on different carbon hexagons. The extended dimers have stabilization energies around 1 eV (1–1.2 eV). When moving the excess hydrogen atoms onto the same carbon hexagon the stabilization energies increase with approximately 0.5 eV to the paradimers (1.4–1.7 eV) and another 0.5 eV to the orthodimers (1.8–2.3 eV). Comparing to GGA-PW91 calculations for hydrogen dimers on graphite, where stabilization energies of only 1.1–1.2 eV are found for short hydrogen dimers,[25] we conclude that edge effects are contributing significantly to the H–H interaction on pyrene.

B. Tight-binding π-band center model

The site preference for the binding of hydrogen on pyrene calculated above in full DFT calculations turns out to be largely predictable at a much lower level of theory. Realizing this starts by noticing that the HOMOs of the pyrene are comprised of the π-system of interacting $2p_z$-orbitals perpendicular to the molecular plane. Once a hydrogen atom binds to a specific carbon atom, a simple assumption would be that the $2p_z$-orbital at that site no longer contributes to any π-orbital of the pyrene, but rather becomes part of a C–H bond. The electronic states at the C site are likely undergoing rehybridization from sp^2 to sp^3 to a large degree, but that is not important for our model.

The purpose of the model is now to predict the site preference for hydrogen binding on pyrene. Assuming that the energy gain of forming the carbon-$2p_z$–hydrogen-$1s$ bond is independent of the site, any site preference must result from the transition of the π-system from being N membered to being $N-1$ membered. In order to evaluate the energy associated with this transition, we resort to a tight-binding framework in which the potential energy of the π-system can be expressed in terms of a sum over eigen energies, e.g.,

$$\begin{aligned} E_\pi &= \sum_n f_n \varepsilon_n \\ &= \sum_n f_n \varepsilon_n \langle \psi_n | \psi_n \rangle \\ &= \sum_J \sum_n f_n \varepsilon_n \langle \psi_n | p_z^J \rangle \langle p_z^J | \psi_n \rangle \\ &= \sum_J \sum_n f_n \varepsilon_n \left| \langle \psi_n | p_z^J \rangle \right|^2, \end{aligned}$$

where n runs over all molecular orbitals, f_n, ε_n, and ψ_n are fillings factors, eigen energies, and molecular orbitals of the nth molecular orbital of the π-system, respectively, and p_z^J is the $2p_z$-orbital on the Jth C-site.

In this model, a simple expression for the stability of the N-membered π-system compared to that of the $N-1$-membered π-system lacking a $2p_z$-orbital at site I can be written

$$\Delta E_\pi^N(I) = E_\pi^N - E_\pi^{N-1:I} \tag{3}$$

$$\begin{aligned} &= \sum_J \sum_n f_n^N \varepsilon_n^N \left| \langle \psi_n^N | p_z^J \rangle \right|^2 \\ &\quad - \sum_{J \neq I} \sum_n f_n^{N-1:I} \varepsilon_n^{N-1:I} \left| \langle \psi_n^{N-1:I} | p_z^J \rangle \right|^2 \\ &\simeq \sum_n f_n^N \varepsilon_n^N \left| \langle \psi_n^N | p_z^I \rangle \right|^2 \equiv \varepsilon_\pi^I, \end{aligned} \tag{4}$$

where superscript N refers to the entire π-system with the $2p_z$-orbital present at site I, and superscript $N-1:I$ refers to the π-system lacking the $2p_z$-orbital at site I. The approximation leading to expression (4) enables the formulation of $\Delta E_\pi^N(I)$ only in terms of the electronic structure *prior* to the removal of the Ith orbital.

The final term, ε_π^I, in Eq. (4) can be interpreted as the energetic mean of the occupied density of states (DOS) projected onto the Ith site, i.e., the *filled π-band center at site I*. This is illustrated in Fig. 6, where densities of states from a tight-binding description of pyrene are shown. The model used is a simple one-parameter tight-binding type Hückel model assuming no overlap between the $2p_z$-basis functions and only nearest neighbor interactions. The on-site interaction (the diagonal elements in the Hamiltonian matrix) is used as energy offset and therefore set to zero. This will make energies of occupied orbitals negative.

In the figure, the left panel shows the total DOS with discrete states being broadened into Gaussians while the middle and right panels depict the densities of states that have been projected (PDOS) on to sites A and D, respectively. The solid horizontal lines show the position of the π-band center and the dashed lines show the lowest and highest occupied π-states, respectively. It is evident that the latter, the HOMO of the π-system, is primarily dominant on site A (raising the

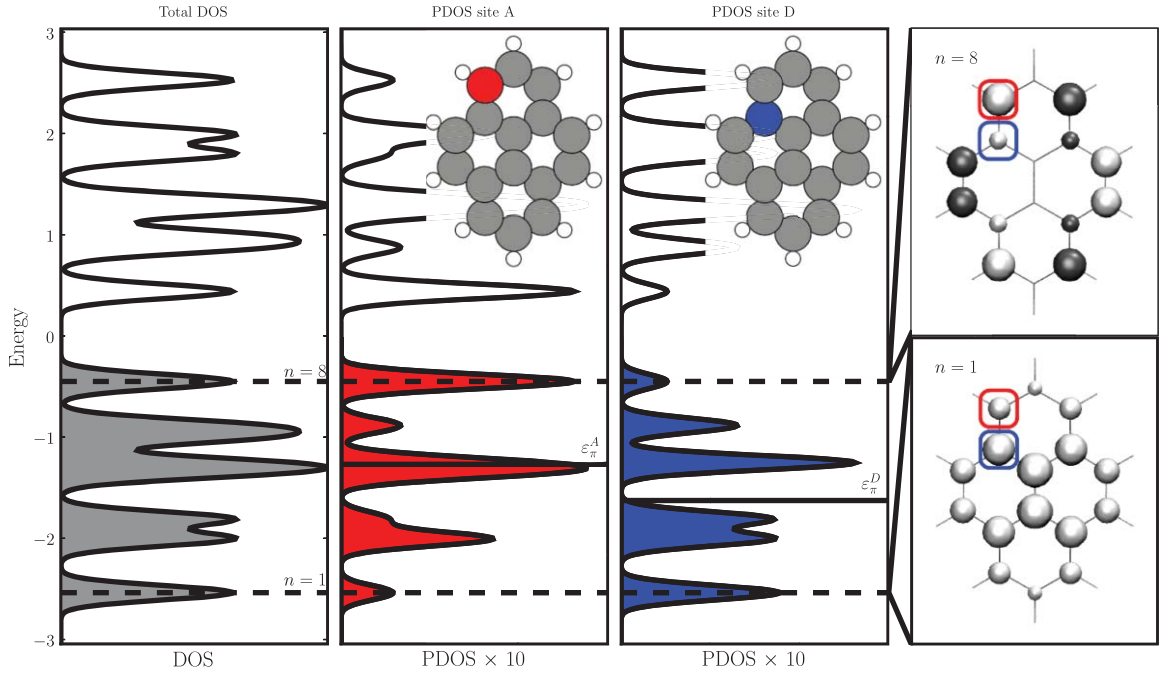

FIG. 6. The left panel shows the total DOS as obtained from the Hückel model. The shaded region is the occupied part. In the two middle panels the PDOS for two different positions (site A and D) are shown and in the plots solid lines indicate the weighted average of the occupied PDOS—the π-band center (ε_π^I). The right panels show as examples the π-orbitals for $n = 8$ (upper) and $n = 1$ (lower). The contributions to the PDOS for site A and D are emphasized by the red and blue squares, respectively. It can be seen how a large weight ($n = 8$ red or $n = 1$ blue) will yield a correspondingly large peak in the PDOS whereas a small weight ($n = 8$ blue or $n = 1$ red) will give rise to a small peak. Effectively, this will give a higher π-band center for position A (red) than for position D (blue). The very stable $n = 1$ orbital collects a big contribution from site D. Because of this it is costly to remove from the π-system the $2p_z$-orbital at this site and therefore less favorable to bond hydrogen at this site as compared with site A. Energies are in units of the absolute value of the tight-binding hopping integral.

π-band center) whereas the former is mostly dominant on site D (lowering the π-band center).

The correlation between DFT based monomer binding energies and the Hückel based π-band center, ε_π^I, is shown in Fig. 7(a). The three most stable binding sites are identified in the right order.

To test the predictive power of the π-band center further, the two most stable monomers are considered and the π-band centers for the formation of dimers from these monomers are determined. The correlation between the DFT based binding energy of the second hydrogen atom and the π-band center is shown in Figs. 7(c) and 7(d). One dimer is not shown since the corresponding DFT calculation did not converge. It is, however, expected to be among the least stable dimers and therefore of little importance.

Generally, the calculated binding energies correlate very well with the π-band center. The most stable dimer created from monomer A and B can be unambiguously anticipated from ε_π and the model gives a good estimate for the next most stable configurations.

Some of the deviations from perfect binding energy/ε_π-correlation can be rationalized. Focusing on Fig. 7(c), the blue points (squares) and the cyan point (left triangle) are found more stable by DFT than predicted by the π-band center. Together with the most stable dimer (red circle) they all have an odd number of bonds between the bonding sites (using the formulation of sublattices from graphene the two hydrogen atoms bond to carbons atoms from different sublattices).

Making a dimer can be considered as two consecutive bindings of a hydrogen atom. For each step in the procedure the π-band center can be determined for the binding site. The sum of the π-band centers from the two steps in the creation of a dimer we term the *accumulated π-band center*. In Fig. 8 a strong correlation between the DFT based binding energies and the accumulated π-band center is seen. This means that the accumulated π-band center can be viewed as a measure of the overall stability of a dimer. This will enable comparison between dimers that have no monomers in common—which, for instance, is the case for the two most stable dimers (cf. Fig. 3).

For the accumulated π-band center to be reliable it must to a high extent commute. That is, the accumulated π-band center for dimer XY should approximately be the same as for dimer YX. The error bars in Fig. 8 measure the deviation from commutativity. Points along the horizontal axis are mean values. Generally there is a very good correlation—the two most stable dimers are unambiguously determined in the right order.

To further substantiate the π-band model it has been tested for the bonding of one hydrogen atom on the coronene molecule. In Fig. 7(b) the correlation between the π-band center and the binding energy is shown and it confirms the picture.

There are several ways to improve this model. Either one can improve on the approximations used in the tight-binding scheme leading to Eq. (4) or the used methodology can be improved. For example, the π-band center can be evaluated within DFT. Another example would be to calculate Eq. (3) within the Hückel model, but this improvement would include information from the final system thus diminishing the

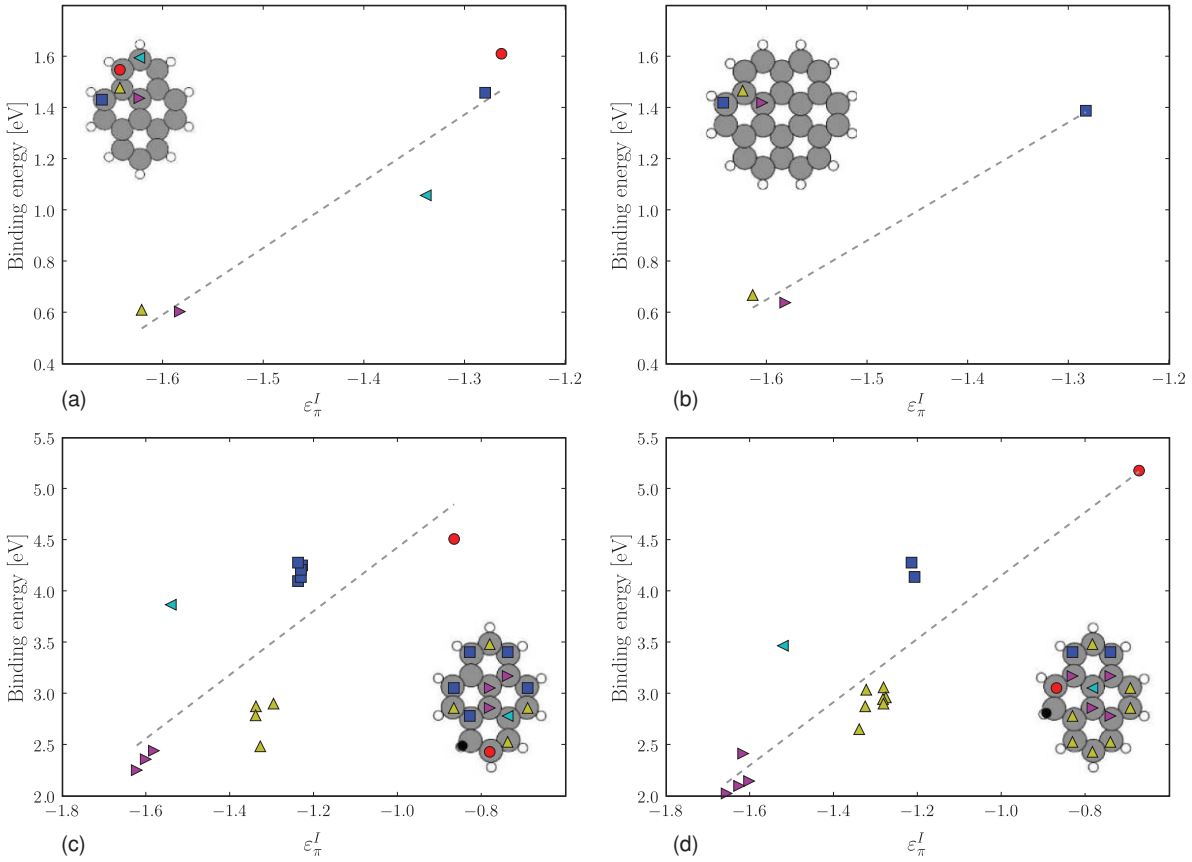

FIG. 7. The correlation between the DFT based binding energies and the Hückel based π-band center for (a): hydrogen monomers on pyrene; (b): hydrogen monomers on coronene; (c): hydrogen dimers on pyrene given monomer A; (d): hydrogen dimers on pyrene given monomer B. The π-band centers are given in units of the absolute value of the tight-binding hopping integral.

simplicity of the model and would suffer from Eq. (3) not being available via DFT. In Fig. 9 is shown how the binding energies for monomers on pyrene correlates with (a): Eq. (3) and with (b): the π-band center Eq. (4) obtained from DFT.

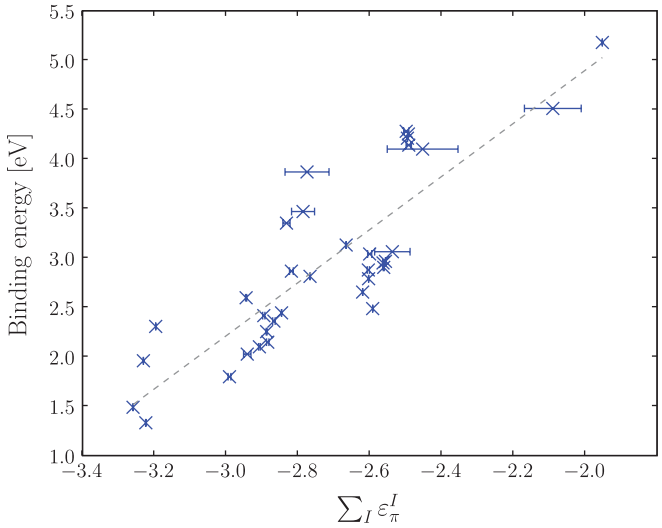

FIG. 8. Correlation between the accumulated π-band center and the total binding energy. Error bars are found by the change in $\sum_I \varepsilon_\pi^I$ upon reverting the binding sequence.

C. Further hydrogenation

In order to analyze whether molecular hydrogen will form or stay bonded on pyrene the thermodynamics of a pyrene molecule in thermal equilibrium with a molecular hydrogen gas has been investigated. In Fig. 10 is shown the free energy for the reaction between pyrene and $N \times \frac{1}{2}H_2$ as a function of the chemical potential of H_2.

Generally—apart from the full hydrogenation—the bonding of two (dimer BB′) and four (tetramer BB′B″B‴) hydrogens are preferred. When these hydrogens are bonded they will not leave—partly due to the endothermicity of the reaction and partly due to a huge kinetic barrier for desorption.

V. HYBRID DFT AND EXACT EXCHANGE

In order to quantify to what extent the calculated results are dependent on the methodology chosen, we repeated selected calculations using either PBE0 or exact exchange. The results for the binding of a hydrogen atom to pyrene with these other methods are given in Table I, while results for the binding of the second hydrogen are reported in Table II. In Table I the binding energies are given as evaluated in two different computational codes, the GPAW and VASP, and some VASP results are further given including structural relaxation within the PBE0 method. It is seen that the GPAW and VASP codes give very similar results, thereby validating the more

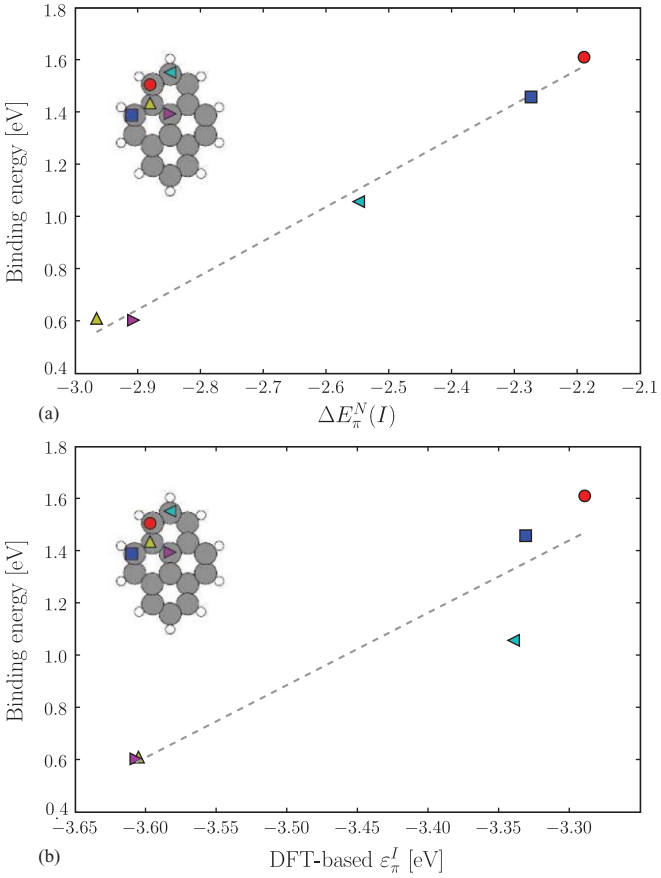

FIG. 9. The correlation between the DFT binding energies and (a): $\Delta E_\pi^N(I)$ of Eq. (3) as obtained from the Hückel model (in units of the hopping integral); (b): the π-band center evaluated within DFT (in eV).

recent PBE0 implementation in the GPAW code.[33,34,47] It is further seen that whether PBE or PBE0 is used when performing the structural relaxation appears to be of minor importance.

Comparing across the tables for each configuration and one given computer code, it is seen that the PBE0 hybrid functional gives results quantitatively comparable with PBE with no significant exceptions. The EXX Hartree–Fock methodology on the other hand leads to evaluation of much stronger binding energies (compared to PBE and PBE0) and reverses the order of monomer D and E.

Comparing in Table II the binding energies of the nine dimer configurations with the three methods PBE, PBE0, and

TABLE I. Binding energies of H on pyrene in eV. Values reported in bold are our PBE results obtained with the GPAW code. PBE-geometries are used in all cases except for the VASP-PBE0 values reported in parentheses for which the PBE0 geometries were used.

	PBE		PBE0			EXX	
Conf.	GPAW	VASP	GPAW	VASP		GPAW	VASP
A	**1.61**	1.65	1.60	1.73	(1.72)	2.15	2.43
B	**1.50**	1.50	1.49	1.60	(1.59)	2.08	2.28
C	**1.06**	1.11	1.01	1.15	(1.15)	1.71	2.07
D	**0.61**	0.64	0.62	0.70	(0.69)	1.31	1.42
E	**0.60**	0.63	0.54	0.61	(0.61)	1.37	1.45

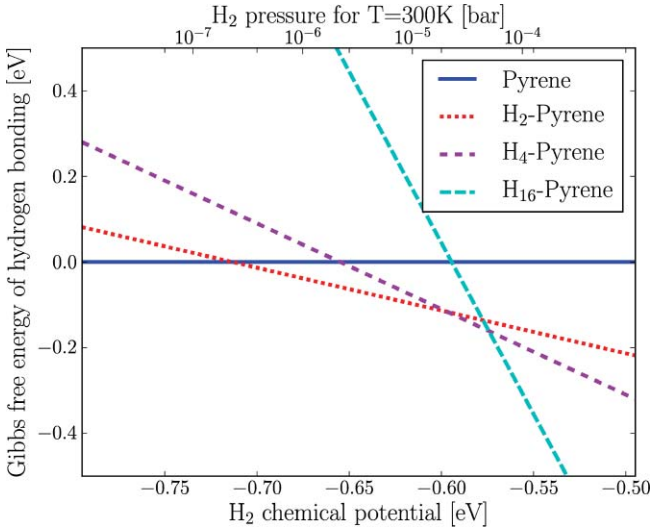

FIG. 10. Gibbs free energy for hydrogen bonding on pyrene as a function of the chemical potential of H_2.

EXX it is seen that the PBE and PBE0 give quantitatively comparable results in all but one case, while the EXX leads to much smaller binding energies as compared to PBE and PBE0. This is also reflected in the stabilization of the hydrogen dimers compared to the monomer binding energies where again the PBE and PBE0 give results that correspond very closely to one another whereas the EXX surprisingly gives negative stabilization energies.

Table III presents the calculated barriers for the bonding of a hydrogen atom to pyrene in the five different positions. The barriers have been calculated both within PBE and PBE0. Calculations with the PBE0 functional show an increase in the barrier for the most and the least stable monomer with about 0.08 eV. For the most stable monomer this is more than a doubling of the barrier (from 0.06 to 0.15 eV). No attempt was made at determining barriers within the EXX method. It has been shown elsewhere that the inclusion of exact exchange improves the reaction barriers for hydrogen transfer reactions.[32]

Generally, PBE and PBE0 give comparable results—qualitatively and quantitatively and there is therefore no reason for investigating the inclusion of exact exchange further for these systems.

TABLE II. Binding and stabilization energies of two H atoms on pyrene in eV.

	Binding energy			Stabilization energy		
Conf.	PBE	PBE0	EXX	PBE	PBE0	EXX
BB′	**5.18**	5.27	4.08	*2.26*	2.28	−0.08
AC	**4.51**	4.48	3.06	*1.84*	1.86	−0.79
AB″	**4.28**	4.27	2.96	*1.21*	1.17	−1.27
AA′	**4.25**	4.20	2.77	*1.03*	1.00	−1.53
AA″	**4.21**	4.17	2.77	*0.99*	0.97	−1.53
AB′	**4.14**	4.12	2.75	*1.07*	1.03	−1.48
AD	**4.10**	4.14	2.96	*1.88*	1.91	−0.50
AD‴	**3.87**	3.91	2.74	*1.65*	1.68	−0.72
BE′	**3.47**	3.42	2.13	*1.41*	1.39	−1.32

TABLE III. Reaction barriers for binding one hydrogen on pyrene in eV.

Conf.	$E_{a,PBE}$	$E_{a,PBE0}$	ΔE_a
A	**0.06**	0.15	0.09
B	**0.08**	0.16	0.08
C	**0.12**	0.25	0.14
D	**0.27**	0.32	0.05
E	**0.24**	0.32	0.08

VI. CONCLUSION

The reactivity of pyrene with respect to hydrogen has been thoroughly established with density functional theory. Furthermore, a model has been presented that can predict the most stable structures of hydrogen on polycyclic aromatic hydrocarbons. The model originates in a very simple one-parameter tight-binding framework making predictions from the model essentially free in terms of computational time. This makes the model very attractive as a screening method pointing out structures to be investigated with density functional theory. The model emphasizes the center of the π-band as an important electronic factor determining the reactivity of these species.

ACKNOWLEDGMENTS

We are indebted to Liv Hornekær for many fruitful discussions. The work was supported by the Danish Ministry of Science, Technology and Innovation through the iNANO center, the Danish Research Councils, the Niels Bohr Foundation, and the Danish Center for Scientific Computing.

[1] D. Hollenbach and E. E. Salpeter, Astrophys. J. **163**, 155 (1971).
[2] E. Habart, F. Boulanger, L. Verstraete, C. M. Walmsley, and P. des Forets, Astron. Astrophys. **414**, 531 (2004).
[3] N. Katz, I. Furman, O. Biham, V. Pirronello, and G. Vidali, Astrophys. J. **522**, 305 (1999).
[4] C. W. Bauschlicher, Astrophys. J. Lett. **509**, L125 (1998).
[5] E. Rauls and L. Hornekær, Astrophys. J. **679**, 531 (2008).
[6] J. L. Puget and A. Leger, Annu. Rev. Astron. Astrophys. **27**, 161 (1989).
[7] J. A. Sebree, V. V. Kislov, A. M. Mebel, and T. S. Zwier, J. Phys. Chem. A **114**, 6255 (2010).
[8] K. May, B. V. Unterreiner, S. Dapprich, and R. Ahlrichs, Phys. Chem. Chem. Phys. **2**, 5089 (2000).
[9] P. Ruffieux, O. Gröning, P. Schwaller, L. Schlapbach, and P. Gröning, Phys. Rev. Lett. **84**, 4910 (2000).
[10] A. J. H. M. Meijer, A. J. Farebrother, D. C. Clary, and A. J. Fisher, J. Phys. Chem. A **105**, 2173 (2001).
[11] X. Sha and B. Jackson, Surf. Sci. **496**, 318 (2002).
[12] X. Sha, B. Jackson, and D. Lemoine, J. Chem. Phys. **116**, 7158 (2002).
[13] Y. Ferro, F. Marinelli, and A. Allouche, J. Chem. Phys. **116**, 8124 (2002).
[14] T. Zecho, A. Güttler, X. Sha, B. Jackson, and J. Küppers, J. Chem. Phys. **117**, 8486 (2002).
[15] Y. Ferro, F. Marinelli, and A. Allouche, Chem. Phys. Lett. **368**, 609 (2003).
[16] R. Martinazzo and G. F. Tantardini, J. Chem. Phys. **124**, 124702 (2006).
[17] L. Hornekær, E. Rauls, W. Xu, Z. Šljivančanin, R. Otero, I. Stensgaard, E. Lægsgaard, B. Hammer, and F. Besenbacher, Phys. Rev. Lett. **97**, 186102 (2006).
[18] L. Hornekær, Z. Šljivančanin, W. Xu, R. Otero, E. Rauls, I. Stensgaard, E. Lægsgaard, B. Hammer, and F. Besenbacher, Phys. Rev. Lett. **96**, 156104 (2006).
[19] L. Hornekær, W. Xu, R. Otero, E. Lægsgaard, and F. Besenbacher, Chem. Phys. Lett. **446**, 237 (2007).
[20] Y. Ferro, D. Teillet-Billy, N. Rougeau, V. Sidis, S. Morisset, and A. Allouche, Phys. Rev. B **78**, 085417 (2008).
[21] D. W. Boukhvalov, M. I. Katsnelson, and A. I. Lichtenstein, Phys. Rev. B **77**, 035427 (2008).
[22] H. M. Cuppen and L. Hornekær, J. Chem. Phys. **128**, 174707 (2008).
[23] J. Kerwin and B. Jackson, J. Chem. Phys. **128**, 084702 (2008).
[24] S. Casolo, O. M. Løvvik, R. Martinazzo, and G. F. Tantardini, J. Chem. Phys. **130**, 054704 (2009).
[25] Z. Šljivančanin, E. Rauls, L. Hornekær, W. Xu, F. Besenbacher, and B. Hammer, J. Chem. Phys. **131**, 084706 (2009).
[26] J. A. Fürst, T. G. Pedersen, M. Brandbyge, and A. P. Jauho, Phys. Rev. B **80**, 115117 (2009).
[27] R. Caballol, J. Igual, F. Illas, and J. Rubio, Surf. Sci. **149**, 621 (1985).
[28] L. Jeloaica and V. Sidis, Chem. Phys. Lett. **300**, 157 (1999).
[29] N. Rougeau, D. Teillet-Billy, and V. Sidis, Chem. Phys. Lett. **431**, 135 (2006).
[30] A. D. Becke, J. Chem. Phys. **98**, 1372 (1993).
[31] J. P. Perdew, M. Ernzerhof, and K. Burke, J. Chem. Phys. **105**, 9982 (1996).
[32] B. J. Lynch, P. L. Fast, M. Harris, and D. G. Truhlar, J. Phys. Chem. A **104**, 4811 (2000).
[33] J. J. Mortensen, L. B. Hansen, and K. W. Jacobsen, Phys. Rev. B **71**, 035109 (2005).
[34] J. Enkovaara, C. Rostgaard, J. J. Mortensen, J. Chen, M. Dułak, L. Ferrighi, J. Gavnholt, C. Glinsvad, V. Haikola, H. A. Hansen, H. H. Kristoffersen, M. Kuisma, A. H. Larsen, L. Lehtovaara, M. Ljungberg, O. Lopez-Acevedo, P. G. Moses, J. Ojanen, T. Olsen, V. Petzold, N. A. Romero, J. Stausholm-Møller, M. Strange, G. A. Tritsaris, M. Vanin, M. Walter, B. Hammer, H. Häkkinen, G. K. H. Madsen, R. M. Nieminen, J. K. Nørskov, M. Puska, T. T. Rantala, J. Schiøtz, K. S. Thygesen, and K. W. Jacobsen, J. Phys.: Condens. Matter **22**, 253202 (2010).
[35] P. E. Blöchl, Phys. Rev. B **50**, 17953 (1994).
[36] J. P. Perdew, K. Burke, and M. Ernzerhof, Phys. Rev. Lett. **77**, 3865 (1996).
[37] C. Adamo and V. Barone, J. Chem. Phys. **110**, 6158 (1999).
[38] G. Henkelman, B. P. Uberuaga, and H. Jónsson, J. Chem. Phys. **113**, 9901 (2000).
[39] G. Henkelman and H. Jónsson, J. Chem. Phys. **113**, 9978 (2000).
[40] J. J. Mortensen, Y. Morikawa, B. Hammer, and J. K. Nørskov, J. Catal. **169**, 85 (1997).
[41] G. Kresse and J. Hafner, Phys. Rev. B **48**, 13115 (1993).
[42] G. Kresse, Comp. Mat. Sci. **6**, 15 (1996).
[43] G. Kresse and J. Furthmüller, Phys. Rev. B **54**, 11169 (1996).
[44] T. P. M. Goumans and J. Kästner, Angew. Chem., Int. Ed. **49**, 7350 (2010).
[45] S. Morisset, F. Aguillon, M. Sizun, and V. Sidis, J. Phys. Chem. A **108**, 8571 (2004).
[46] D. Teillet-Billy, N. Rougeau, V. V. Ivanovskaya, and V. Sidis, Int. J. Quantum Chem. **110**, 2231 (2010).
[47] C. Rostgaard, Master's thesis, Technical University of Denmark, 2006.